Journal of Computer-Aided Molecular Design, **13:** 315–324, 1999.
KLUWER/ESCOM

Electron-density-dependent fused-sphere surfaces derived from pseudopotential calculations

Gustavo A. Arteca[a,*] & Naomi D. Grant[b]
[a]*Département de Chimie et Biochimie and* [b]*Department of Biology, Laurentian University, Ramsey Lake Road, Sudbury, ON, Canada P3E 2C6*

Received 7 July 1998; Accepted 6 October 1998

Key words: atomic radii, isodensity contour surface, LANL2DZ basis set, molecular shape, molecular surface

Summary

Fused-sphere surfaces can be used to mimic a molecular 'boundary' associated with a constant value of the electron density. The simplest of such fused-sphere models are constructed by using the atomic radii for the spherical isodensity surfaces of individual atoms. In this work, we discuss the extension of this model to molecules containing atoms beyond the second row. In these many-electron systems, the computation of electron densities is usually simplified by adopting a *pseudopotential* (or effective-core potential) approach. Here, we discuss the performance of large- and small-core pseudo-potential calculations as a tool to derive atomic radii. Our results provide an optimum set of variable radii that can be used to build fused-sphere surfaces. This continuum of surfaces provides a simple approximation to the low-electron-density regions around molecules with heavy atoms.

Introduction

Most molecular modelling techniques associate a boundary surface to a molecule [1,2]. A boundary allows one not only to compute the volume and surface area, but also to map physical properties in the neighbourhood of a molecule [3]. More realistic models often employ a *continuum of electron isodensity contours* to introduce a 'fuzziness' in the boundary. When seeking to reduce computer time, these contours can be modelled by 'patching' together smaller pieces assumed to be transferable. In this work, we discuss a version of this approach to building surfaces that can be employed in molecules with heavy atoms.

A great deal of effort has been devoted to developing methods that compute the *molecular* electron density function, $\rho(\mathbf{r})$, from the electron densities of smaller sub-molecular pieces. Some approaches include: (i) the evaluation of the electron density for a quantum subsystem [4]; (ii) partitioning schemes in density functional theory [5]; (iii) the superposition of local Gaussian electron densities [6,7]; and (iv) the direct addition of the electron densities of pre-set chemical neighbourhoods (e.g., functional groups) [8].

In the simplest scheme using transferable pieces, each atom is assigned a fixed contribution to $\rho(\mathbf{r})$ regardless of its environment. The resulting electron densities are not accurate for computing expectation values. However, the method provides a convenient representation of a surface that can be used in molecular similarity analyses [9]. In fact, properties of these surfaces (e.g., their area and volume) are known to correlate well with observables such as relative solubilities, viscosities, and critical parameters [10–14].

Fused-sphere (or 'hard-sphere') *surfaces* are common models built from *fixed atomic pieces*. Such models include the familiar van der Waals and solvent accessible surfaces [1], whose construction relies on a set of atomic radii. Several criteria have been proposed to derive atomic radii from the electron density, using, e.g., the integrated electronic charge or molecular volume, conformationally invariant cores, and properties of the electrostatic potential [7,15–25] (for a comparison, see references 17, 24, and 25). In this work, we deal with the construction of a continuum

*To whom correspondence should be addressed. Present address: Fysikalisk kemiska Institutionen, Uppsala University, Box 532, S-751 21 Uppsala, Sweden.

of fused-sphere surfaces, rather than a single van der Waals surface. Such a continuum is defined by variable atomic radii dependent on the electron density. These radii allow one to model molecular surfaces that mimic *different regimes* of the electron density. Important regimes comprise the region consistent with the empirical molecular volume [4,16] (i.e., $\rho(\mathbf{r}) \approx 2 \times 10^{-3}$ a.u.), as well as outer 'layers' involved in molecular recognition (e.g., $\rho(\mathbf{r}) \leq 10^{-4}$ a.u.). (Note that 1 a.u. $= e/a_0^3$, where e is the absolute value of the electron charge and a_0 is the Bohr radius.)

A set of atomic radii dependent on the electron density has been proposed for 'light' elements [17]. In the present work, we discuss an extension of this approach to molecules containing second- and third-row elements. In this case, the construction of the electron density is greatly simplified by using *pseudopotentials* or *effective-core potentials* (ECP) [26–28]. Pseudopotentials are based on the notion that inner (core) electrons are inert, changing little when forming a molecule. Accordingly, one can replace the core electrons by an effective interaction, thereby reducing the number of electrons to those in the valence shell. This approach has been highly successful to analyze a number of properties of molecules containing transition metals [27, 28].

Effective-core potentials can be used to measure molecular size. For instance, pseudopotential orbital radii correlate with properties such as polarizabilities, electronegativity, and atomic hardness [18, 22, 29]. (Orbital radii depend on angular momentum, and they are defined by the classical turning points of the effective potential [30].) In this work, we deal with the performance of ECPs as tools to build fused-sphere models over a relevant range of electron densities. In particular, we are interested in comparing the performance of pseudopotential and all-electron methods for building molecular surfaces over chemically relevant boundaries, e.g., where the electron density is $\rho(\mathbf{r}) < 5 \times 10^{-3}$ a.u. This is a nontrivial comparison, since the latter range of electron density is associated with a region where the core cannot, in principle, be ignored. Accordingly, the reliability of a constant electron density contour derived from pseudopotentials is not guaranteed.

The work is organized as follows. In the next section, we discuss the performance of ECPs to compute electron-density-dependent atomic radii for second-row elements. The pseudopotential approach is compared with ab initio all-electron calculations. In a following section, ECPs are used for third-row elements, for which standard all-electron Gaussian basis sets are not available. In this case, we provide a consistent set of atomic radii that can be used for building fused-sphere models that resemble isodensity contours. The last section discusses the physical significance of a van der Waals boundary surface, as well as the limitations of the pseudopotential approach in computing atomic radii.

Electron-density-dependent atomic radii

Let $\rho(\mathbf{r})$ be the one-electron density (i.e., a fractional charge per unit of volume around a point $\mathbf{r}$), obtained by integrating the total density over all electrons but one. Within the unrestricted Hartree-Fock (UHF) approach for open-shell configurations, the electron density $\rho(\mathbf{r})$ can be written in terms of atomic orbitals $\{\phi_\mu\}$ as follows:

$$\rho(\mathbf{r}) = \sum_\mu \sum_\nu (P_{\mu\nu}^{(\alpha)} + P_{\mu\nu}^{(\beta)}) \phi_\mu(\mathbf{r})\, \phi_\nu^*(\mathbf{r}), \qquad (1)$$

where $P_{\mu\nu}^{(\alpha)}$ and $P_{\mu\nu}^{(\beta)}$ represent the density matrices for α- and β-electrons, respectively. In this work, we have calculated UHF electron densities for ground states (with the largest spin multiplicity). All calculations have been carried out with the ab initio package Gaussian 92 (Revision G.4) [31], running on a DEC (Alphaserver) 3000 Model 400.

In order to build a fused-sphere model that mimics an isodensity contour, it is convenient to use an 'inverted' representation, i.e., one where the radius r of a spherical shell can be computed for a given ρ value. Consequently, we have derived numerical expressions of the form $r = r(\rho)$, valid over a range of densities consistent with the condition $r > R_{core}$, where R_{core} is approximately the radius of the invariant inner-electron core. (For the present analysis, the actual value of R_{core} is not important. Ultimately, the choice of R_{core} will be dictated by the range of r values over which the desired functional form for $r(\rho)$ produces the best numerical fittings. As a conservative estimate, we can take $R_{core} \sim 1.0$ Å for first- and second-row elements, and $R_{core} \sim 1.5$ Å for third-row elements.) Since the atomic one-electron density falls exponentially for large atomic radii, we assume a behaviour of the form:

$$\rho(r) = f(r)\, e^{-\zeta(z)r}, \; r > R_{core}, \qquad (2)$$

where $f(r)$ is a polynomial of r. If this general function is developed in Taylor series about a constant,

$r > R_{core}$, then a variable such as $x = \log \rho(r)$ can be represented as a truncated expansion in powers of r. By inverting this expansion, we can express the atomic radii $r > R_{core}$ as a series of x [17]:

$$r = \sum_{s \geq 0} c_s x^s, \; r > R_{core} \tag{3}$$

In the next sections, we use a uniform description for the radii of second- and third-row elements, where r is fitted as a second-degree polynomial, $r(x) \approx c_0 + c_1 x + c_2 x^2$. As we show in the next section, this approach is sufficiently accurate for the goals of this work. In order to compare the various computational approximations to the electron density, we perform this fitting by using the same electron density values for atoms within a given row of the periodic table.

It must be noted that a second-degree polynomial is a proper fitting for *r(x) only for low electron density values*, i.e., in spherical regions far from the nuclei. Accordingly, our *r(x)* expressions cannot be used to study covalent radii, which satisfy $r < R_{core}$ (typically 0.7 Å and 1.0 Å for first- and second-row elements, respectively). Nonetheless, the present approach is appropriate for studying van der Waals radii, denoted by σ, whose empirical values appear to satisfy $\sigma > R_{core}$. Below, we shall use the equality $r(x) = \sigma$ to relate the van der Waals radii with values of the electron density ($\rho = 10^x$). As a result, we derive a set of atomic radii that can be used to build a van der Waals surface that mimics an isodensity molecular boundary.

Performance of pseudopotential methods for atomic radii of second-row elements

Our first goal is to compare the results for *r(x)* in light atoms, computing the one-electron density with: (i) an ab initio UHF approach including all electrons; (ii) a small-core pseudopotential approach; and (iii) a large-core pseudopotential approach. All-electron UHF densities for first- and second-row atoms have been evaluated with the 3-21G* and 6-31G** basis sets. Gaussian basis sets are available for pseudopotential calculations (see discussions in References 32–34). In our case, we will compare the performance of the methods that combine valence-electron orbitals with large-core [32] and small-core [33] effective potentials. (Within the context of standard computational chemistry packages, ECPs are the only 'ab initio' approaches available for molecules with third-row atoms. In Gaussian 92, the large- and small-core pseudopotential basis sets appear under the codes LANL1DZ and LANL2DZ, respectively [31]. We shall use the generic notation LANLxDZ to indicate the cases where the two approaches are identical. In our present goal of deriving reliable electron density *contour surfaces*, we will restrict ourselves to employing these readily available basis sets. However, for a number of *integrated* electron density properties, more extended basis sets may be needed. A particularly convenient, general approach to deriving effective-core potentials and extended valence basis sets is given in Reference 35. This method is applied to transition metals and lantanides in References 36 and 37.)

Pseudopotential methods replace the all-electron configuration by an effective core and valence electrons. The choice of the 'core' is dictated by a compromise between computational expediency and precision. The large-core ECPs allow faster calculation, but they are known to provide deficient integrated electron density properties [38]. However, it is still possible that they provide reasonable atomic radii to build molecular boundaries. We test this conjecture in the next section.

For first- and second-row elements (Li–Ar), there is no difference between a small and a large core. Differences are found in alkalines, earth alkalines and transition metals in rows $n \geq 3$. A small-core potential partitions the electronic configuration as follows:

$$[\textit{small-core}](n+1)s^2(n+1)\mathrm{p}^6 \\ (n+1)\mathrm{d}^{\mathrm{m}}(n+2)\mathrm{s}^{\mathrm{q}}, \tag{4}$$

for the elements *up to* $\mathrm{m} + \mathrm{q} = 12$. (Note that n denotes the *row index* in the periodic table.) On the other hand, a large-core potential incorporates s and p electrons into the core:

$$[\textit{large-core}](n+1)\mathrm{d}^{\mathrm{m}}(n+2)\mathrm{s}^{\mathrm{q}}. \tag{5}$$

Once the $(n+1)$d and $(n+2)$s electrons are filled, there is no longer any difference between large and small cores. In other words, we expect no difference in the two ECP schemes for the series of third-row elements Ga–Br.

Figure 1 presents a representative result for first-row elements, taking carbon as an example. The figure compares the spherical radius r of carbon as a function of the electron density derived with UHF and pseudopotential methods. The results are virtually indistinguishable for electron densities $\rho > 4 \times 10^{-4}$ a.u., which corresponds approximately to $r <$

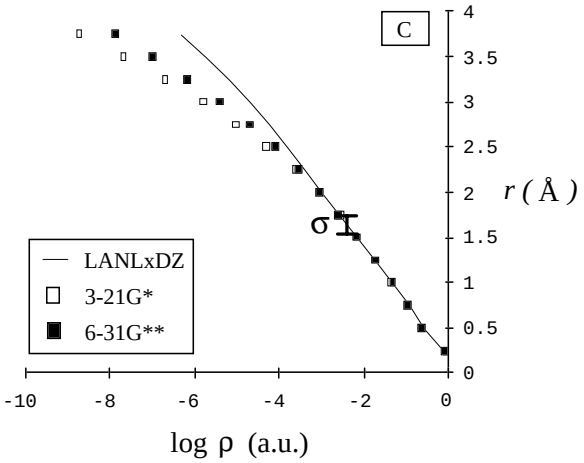

Figure 1. Dependence of the atomic radius of carbon on its electron density, computed at the ab initio UHF level, using different basis sets and effective-core potentials. (The bar indicates the range of densities associated with the *empirical* van der Waals radius σ. The value of σ for carbon is used as reference for all other atoms.)

2.0 Å. The standard van der Waals radius of carbon (denoted by σ(C)) is found in this range: 1.60 Å ≤ σ(C) ≤ 1.75 Å [39, 40].

In this work, we choose carbon as a *reference atom*. Accordingly, we obtain the electron density value associated with its empirical van der Waals radius (i.e., a 'reference electron density') and then use this electron density value to compute the radii for other elements. It must be stressed that the choice of the reference atom is not too critical for the results in this work. As shown in Reference 17, by choosing the empirical van der Waals radius of carbon as a reference, one obtains atomic radii for the other first-row elements that are consistent with their empirical van der Waals radii. Accordingly, similar results would be obtained by using the well-established van der Waals radii of oxygen or nitrogen as a reference. Note, however, that hydrogen does not provide a convenient reference, since its van der Waals radius is characterized with a large uncertainty range: 1.00 Å ≤ σ(H) ≤ 1.30 Å [17, 39, 40].

For the determination of the 'reference' (or 'boundary') electron density range, we proceed as follows. A fitting of the UHF/3-21G* electron density of carbon in Figure 1 over the range of values $r \in$[1.0 Å, 3.5 Å] (a total of 11 points) produces:

$$r_{3-21G^*} \approx (0.152 \pm 0.046) - (0.695 \pm 0.024)x - (0.034 \pm 0.003)x^2, \quad (6a)$$

with a correlation coefficient $\mathcal{C} = 0.99945$ and 95% confidence intervals. Using this function, the range of electron density consistent with $r = \sigma(C) = 1.675 \pm 0.075$ Å is found to be $\rho_{3-21G^*} = 0.0033 \pm 0.0011$ a.u. A similar calculation in the UHF/6-31G** scheme produces the following fitting over the same range of atomic radii:

$$r_{6-31G^{**}} \approx (0.076 \pm 0.020) - (0.729 \pm 0.011)x - (0.035 \pm 0.001)x^2, \quad (6b)$$

with a correlation coefficient $\mathcal{C} = 0.99991$. In this case, the range of electron densities associated with the reference value σ(C) is $\rho_{6-31G^*} = 0.0034 \pm 0.0010$ a.u. Finally, a similar fitting with the pseudopotential (UHF/LANLxDZ) approach gives:

$$r_{\mathrm{LANLxDZ}} \approx (0.073 \pm 0.038) - (0.692 \pm 0.023)x - (0.016 \pm 0.003)x^2, \quad (6c)$$

with a correlation coefficient $\mathcal{C} = 0.99980$. Here, the reference radius σ(C) leads to a range of electron density $\rho_{\mathrm{LANLxDZ}} = 0.0036 \pm 0.0010$ a.u., which is close to those obtained in all-electron UHF approaches. (This range is denoted in Figure 1 with the symbol 'σ'. It is worth mentioning that our ρ_{LANLxDZ} value is larger than the other commonly used boundary, $\rho = 2 \times 10^{-3}$ a.u., proposed in Reference 16 to match the empirical molecular volumes. Note, however, that a change in electron density from 3×10^{-3} a.u. to 2×10^{-3} a.u. increases all the atomic radii rather uniformly only by a factor of less than 10% [17]. This difference in 'boundary' electron density does not affect the main conclusions in our work.)

Note that, in all cases, the quality of the fitting to a second-degree polynomial seems adequate to produce a reliable interpolation of electron densities. We have checked the robustness of the derived ranges of electron density by re-fitting r versus x as a third-degree polynomial. Even though the $\{c_s\}$ coefficients vary (Equation 3), the conclusions do not change. For example, a fitting of the UHF/3-21G* electron density of carbon gives: $r_{3-21G^*} \approx -(0.097 \pm 0.027) - (0.921 \pm 0.023)x - (0.092 \pm 0.006)x^2 - (0.0043 \pm 0.0004)x^3$, with $\mathcal{C} = 0.99997$. With this result, the electron density range consistent with the van der Waals radius of carbon becomes: $\rho_{3-21G^*} = 0.0036 \pm 0.0011$ a.u. Similarly, the fitting to third-degree polynomials of the UHF/6-31G** and UHF/LANLxDZ electron densities produces $\rho_{6-31G^*} = 0.0035 \pm 0.0011$ a.u. and $\rho_{\mathrm{LANLxDZ}} = 0.0034 \pm 0.0009$ a.u., respectively.

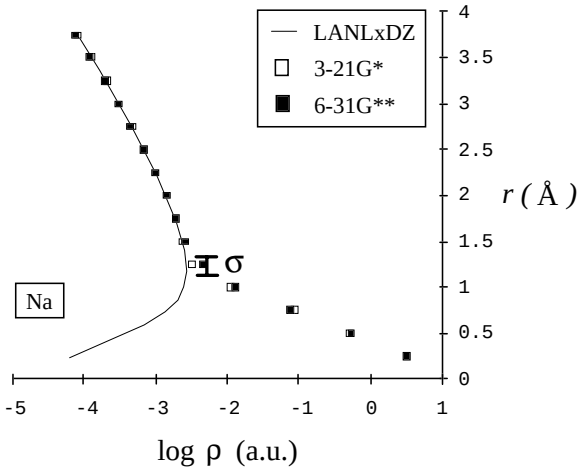

Figure 2. Dependence of the atomic radius of sodium on its electron density, computed at the ab initio UHF level, using various basis sets and effective-core potentials. (The pseudopotential approach cannot be used to define a van der Waals radius σ.)

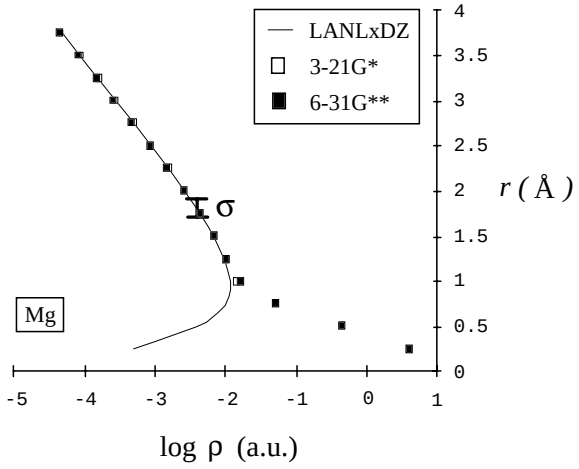

Figure 3. Dependence of the atomic radius of magnesium on its electron density, computed at the ab initio UHF level, using various basis sets and effective-core potentials. (Here the pseudopotential approach provides a good description of the electron density within a region comparable to the van der Waals radius σ.)

Summarizing, the three approaches above indicate consistently that a spherical contour $\rho \sim 3 \times 10^{-3}$ a.u. has a radius equal to σ(C). We can now use the electron densities ρ_{3-21G^*}, $\rho_{6-31G^{**}}$, and $\rho_{LANLxDZ}$ to derive the corresponding van der Waals radii for other second-row elements (denoted by σ_{3-21G^*}, $\sigma_{6-31G^{**}}$, $\sigma_{LANLxDZ}$, respectively), and thus assess the performance of ECP methods to compute atomic radii $r(x)$ for the series Na–Cl.

The limitations of the pseudopotential approach become apparent in Figure 2, showing the results for Na. In this case, the ECP-derived electron density matches the all-electron result *only* for $r > 1.5$ Å. For radii closer to the effective core, the ECP-derived electron density is too low. Since the maximum ρ value ($\rho \approx 10^{-3}$ a.u.) is below the reference electron density ($\rho_{LANLxDZ} = 0.0036$ a.u.), we conclude that the ECP approach cannot be used to compute a (carbon-reference) van der Waals radius for Na. The van der Waals radius (denoted by σ in Figure 2) can still be computed when all electrons are used.

For other second-row elements, the pseudopotential approach is satisfactory. Figure 3 shows the results for Mg. In this case, the ECPs provide an excellent match for the ab initio electron density in the range $\rho < 10^{-2}$ a.u. The same quantitative agreement is found for Al, Si, P, and S. The ECP approach is less accurate in the case of Cl, where the electron density is underestimated for $r > 2.5$ Å (see Figure 4). However, the van der Waals radius computed at the reference electron density ($\rho_{LANLxDZ} = 0.0036$ a.u.) is still in close agreement with the ab initio results. Table 1 collects the results for the atomic radii of second-row elements derived from the reference electron densities. (The errors in σ are determined by the uncertainty range in the reference density $\rho_{LANLxDZ}$.) Except for the failure in Na, the pseudopotential approach provides results virtually indistinguishable from those obtained with the full UHF electron density. In the next section, we discuss the computation of atomic radii for third-row elements.

Electron-density-dependent atomic radii for third-row elements

Split-valence basis sets for all-electron calculations are not available for third-row elements. For this reason, we rely on electron densities for pseudopotential calculations. In this section, we compare the performance of small- and large-core pseudopotentials for the evaluation of atomic radii.

Figure 5 shows the results for K (top) and Ca (bottom). These two elements provide a critical test for the performance of ECP methods. Figure 5 compares the results obtained with a small-core potential (LANL2DZ basis set) and those derived with a large-core potential (LANL1DZ basis set). The following observations can be made:

(i) The large-core pseudopotential fails to produce a van der Waals radius for K, since we find $\rho <$

Table 1. Van der Waals radii for second-row elements, computed at the reference electron density determined by the carbon radius σ(C), using different basis sets

Element	Radii (Å), σ_{3-21G^*} [$(3.3 \pm 1.1) \times 10^{-3}$ a.u.]	Radii (Å), $\sigma_{6-31G^{**}}$ [$(3.4 \pm 1.0) \times 10^{-3}$ a.u.]	Radii (Å), $\sigma_{LANLxDZ}$ [$(3.6 \pm 1.0) \times 10^{-3}$ a.u.]
Na	1.31 ± 0.26	1.41 ± 0.25	–
Mg	1.97 ± 0.23	1.86 ± 0.18	1.86 ± 0.18
Al	2.28 ± 0.17	2.24 ± 0.16	2.20 ± 0.16
Si	2.09 ± 0.14	2.05 ± 0.13	2.02 ± 0.12
P	1.89 ± 0.16	1.90 ± 0.10	1.88 ± 0.10
S	1.98 ± 0.10	1.97 ± 0.10	1.95 ± 0.09
Cl	1.85 ± 0.09	1.84 ± 0.09	1.83 ± 0.07

The ranges of electron densities are indicated in brackets. The errors in σ are associated with the uncertainty in the reference electron density. The 'LANLxDZ' symbol indicates that there is no difference in the small- and large-core pseudopotentials for these elements.

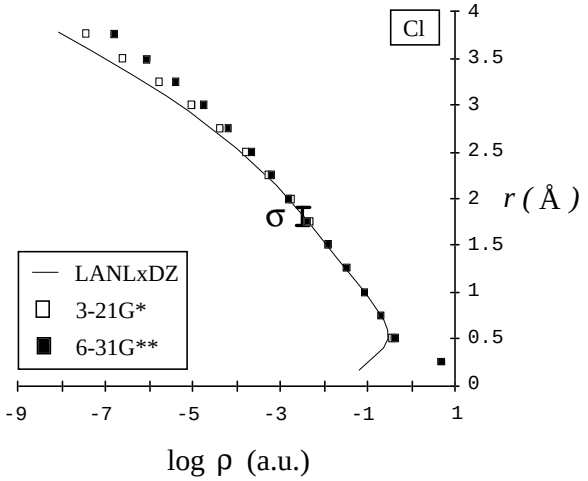

Figure 4. Dependence of the atomic radius of chlorine on its electron density, computed at the ab initio UHF level, using various basis sets and effective-core potentials. (Here the pseudopotential approach provides a good description of the electron density within a region comparable to the van der Waals radius σ, but it deviates systematically for $\rho < 10^{-4}$ a.u.)

$\rho_{LANLxDZ}$ for all r, where $\rho_{LANLxDZ} = 0.0036$ a.u. is the reference density of carbon. (This reference value is indicated by the *horizontal* error bars in σ.)

(ii) The van der Waals radius σ can only be computed for K when using a small-core pseudopotential. However, the region of atomic radii associated with the reference density is poorly described by a quadratic function $r(x)$. Our approximation appears to be reasonable *only* for very low electron densities ($\rho < 10^{-3}$ a.u.).

(iii) Large- and small-core pseudopotentials produce a similar van der Waals radius σ for Ca. Note, however, that the two approximations behave very

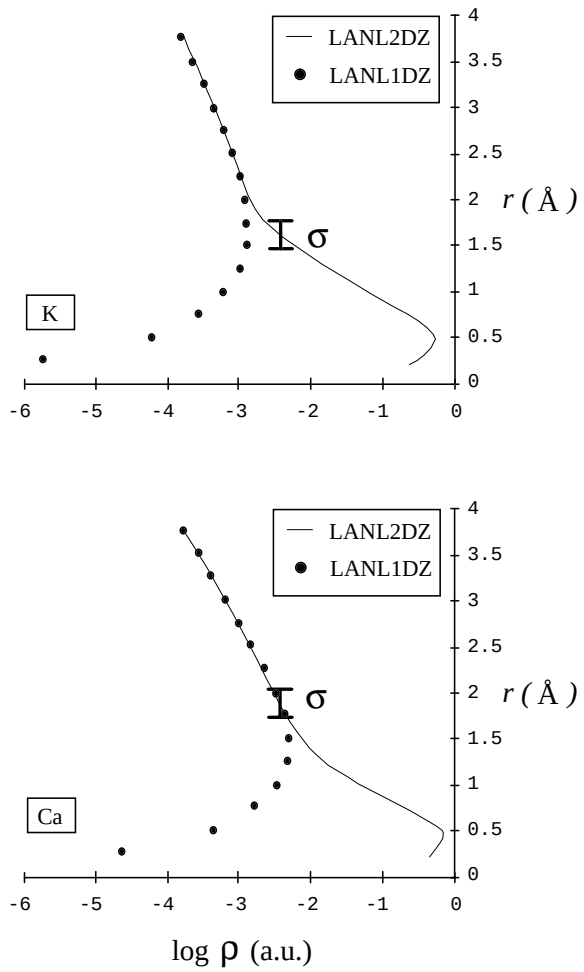

Figure 5. Dependence of the atomic radius of potassium and calcium on the electron density, computed using small- and large-core pseudopotentials. (The large-core pseudopotential (LANL1DZ basis set) cannot be used to estimate a van der Waals radius σ for K.)

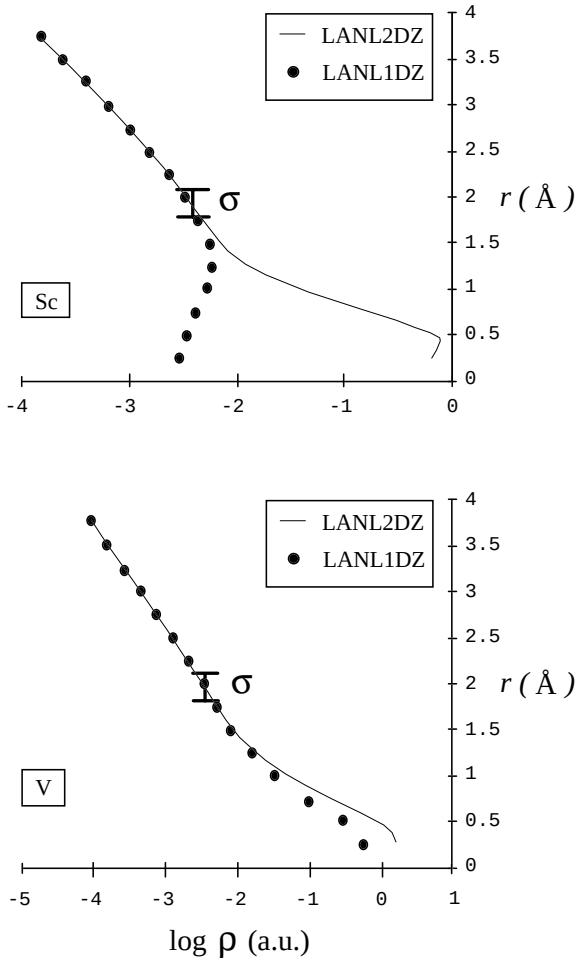

Figure 6. Dependence of the atomic radius of scandium and vanadium on the electron density, computed using small- and large-core pseudopotentials. (The large-core pseudopotential (LANL1DZ basis set) provides a good approximation for the van der Waals radius σ in Sc. The description is even better for V. For third-row elements following V, the results from LANL1DZ and LANL2DZ basis sets are virtually indistinguishable for $\rho < 0.01$ a.u.)

differently for $r < \sigma$. When $r > \sigma$, the two effective cores give nearly identical electron densities, and a quadratic function $r(x)$ represents accurately the atomic radii for densities as low as 10^{-4} a.u.

The situation improves for heavier elements. We note two facts: (i) in the series of elements Sc–Br, van der Waals radii can be defined when using large-core potentials; and (ii) both small- and large-core pseudopotentials provide a description of atomic radii that can be accurately represented as a quadratic function of $x = \log \rho$.

Figure 6 illustrates these findings with two representative examples. The top diagram in Figure 6 shows the results for Sc obtained with the LANL2DZ and LANL1DZ basis sets. The two methods provide similar $r(x)$ functions for $r > \sigma$, where σ is the van der Waals radius at the reference density. The bottom diagram in Figure 6 corresponds to V. In this case, the two pseudopotential approaches describe the same atomic radii for electron density contours satisfying $\rho < 10^{-2}$ a.u., including the van der Waals radius σ obtained at the reference electron density.

Table 2. Van der Waals radii for third-row elements, computed at the reference electron density determined by the carbon radius σ(C), $0.0026 \leq \rho_{\mathrm{LANLxDZ}} \leq 0.0046$ a.u.

Element	Small-core pseudopotential radius σ (Å)	Large-core pseudopotential radius σ (Å)
Ca	1.91 ± 0.21	–
Sc	1.96 ± 0.21	1.90 ± 0.24
Ti	1.90 ± 0.21	1.96 ± 0.19
V	1.95 ± 0.14	1.95 ± 0.17
Cr	1.78 ± 0.13	1.78 ± 0.14
Mn	1.90 ± 0.16	1.91 ± 0.16
Fe	1.81 ± 0.12	1.83 ± 0.11
Co	1.77 ± 0.11	1.71 ± 0.13
Ni	1.73 ± 0.12	1.73 ± 0.11
Cu	1.69 ± 0.12	1.69 ± 0.12
Zn	1.79 ± 0.13	1.79 ± 0.13
Ga	2.18 ± 0.15	2.18 ± 0.15
Ge	2.05 ± 0.13	2.05 ± 0.13
As	1.94 ± 0.10	1.94 ± 0.10
Se	2.04 ± 0.09	2.04 ± 0.09
Br	1.93 ± 0.09	1.93 ± 0.09

The small-core pseudopotential corresponds to the LANL2DZ basis set, whereas the large-core pseudopotential corresponds to the LANL1DZ basis set. The results are identical for elements following Cu. The errors in σ are associated with the uncertainty in the reference electron density.

Large-core pseudopotentials maintain an acceptable performance in elements following V. (As commented before, there is no difference in the small and large cores for elements in the series Zn–Br.) Table 2 completes the comparison by listing the van der Waals radii σ measured with respect to the carbon atom radius (i.e., using the reference electron density $\rho_{\mathrm{LANLxDZ}} = 0.0036 \pm 0.0010$ a.u.). It must be pointed our that, whereas the van der Waals radii computed with small- and large-core ECPs are virtually indistinguishable for most elements, Figures 5 and 6 show that important differences are found in the inner shells.

The radii in Table 2 are in good agreement with the few available empirical van der Waals radii computed from crystal packing, molecular volume, or critical

constants [39–41]. For instance, the van der Waals radius of As is listed as 1.85 Å [39] and 1.94 Å [41], in agreement with our result at the reference density (present value: 1.94 ± 0.10 Å). Similarly, the empirical value for Se is given as 1.90 Å [39] and 2.00 Å [42] (present value: 2.04 ± 0.09 Å), and the value for Br is listed as 1.85 Å [39] and 1.95 Å [42] (present value: 1.93 ± 0.09 Å). Empirical results for σ in transition metals are not available; most common molecular modeling packages assign them, rather arbitrarily, a flat value $\sigma \approx 2.0$ Å. Our results in Table 2 provide an improved approximation based on atomic isodensity surfaces in the context of small-core pseudopotential calculations.

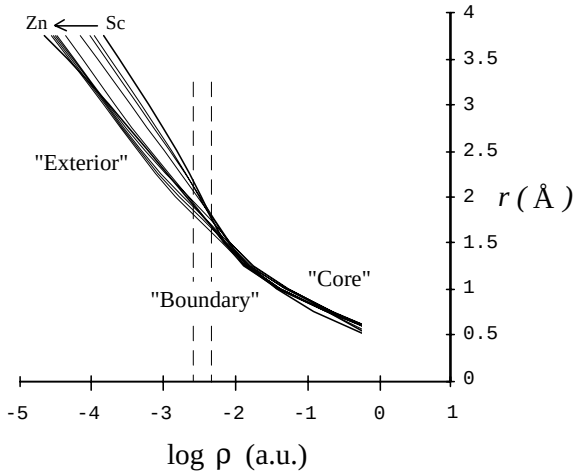

Figure 7. Variable atomic radii for third-row transition metals obtained from small-core pseudopotential electron densities. (The thin lines indicate the results for the elements between Sc and Zn, appearing in the order denoted by the arrow at the top of the diagram. The 'Boundary' region is defined by the reference electron density range within a pseudopotential approach, i.e., $0.0026 \leq \rho \leq 0.0046$ a.u. The upper bound to the boundary density, $\rho_{max} = 0.0046$ a.u., appears to define the limit of the inner core, since there is little difference between the atoms for $\rho > \rho_{max}$. Major differences in atomic sizes appear only in the 'Exterior' region, where $\rho < \rho_{min} = 0.0026$ a.u.)

Further comments and conclusions

In this work, we have shown that small-core pseudopotentials can be used to compute van der Waals radii of third-row elements, whereas large-core pseudopotentials can only be used for elements after Sc. Our results also provide a consistent set of variable atomic radii $\{r(x)\}$, parametrized in terms of the one-electron density ($\rho = 10^x$). For third-row elements, this electron density can be computed at a very low computational cost within the small-core ECP approach, using the LANL2DZ basis set.

Table 3 shows the second-degree polynomial fittings of the atomic radii as a function of the electron density computed with the small-core ECP approach. (The results for first- and second-row elements are valid for $r \in$[1.0 Å, 3.5 Å], whereas the results for third-row elements are valid for $r \in$[1.5 Å, 3.75 Å].) The table indicates that a second-degree polynomial provides a fitting of uniform quality for all third-row elements. With these results, it is now possible to assemble a fused-sphere surface that mimics an isodensity boundary with a desired ρ value. The required atomic radii are determined by Equation 3, the coefficients in Table 3, and the desired x value. (For first-row elements one can simply use the atomic radii computed in Reference 17 with all-electron ab initio methods.) Once a set of atomic radii is defined, the mapping of other physical properties on the molecular surface can be performed more easily than on actual electron-density contours.

Nevertheless, we must strongly stress one point here. The present approach must be regarded as reliable *only* for the restricted goal we set: the derivation of qualitatively acceptable isodensity contour surfaces for molecules with heavy atoms. Our results, based on using standard double-zeta (LANLxDZ) valence basis sets, do not guarantee an electron density that is reliable for the computation of expectation values and other integrated properties. In this latter case, other, more complete, basis sets may be needed [35].

The present results also provide some insights on the physical interpretation of the molecular boundary surface. According to the present definition, the van der Waals radius is completely determined by the electron density of the chosen boundary, without making explicit reference to the shell structure of any particular atom. In other words, we have assumed that the reference boundary surface of carbon provides an electron density value that can also determine a 'meaningful boundary' for other (second- and third-row) atoms. We can now test whether this is a reasonable assumption by looking at our calculations from effective-core potentials.

Figure 7 shows the collected results for the electron densities and atomic radii in third-row transition metals (Sc–Zn), derived with small-core pseudopotentials. (Only the results for $r > 0.5$ Å are displayed.) Since these elements share the same 'small core', there is a range of electron density where atoms cannot be

Table 3. Coefficients $\{c_i\}$ for the expansion of the atomic radii in terms of $x = \log \rho$, where ρ is the electron density calculated with the small-core pseudopotential LANL2DZ basis set

Element	c_0	c_1	c_2	$\mathcal{C}$
C	0.073 ± 0.038	-0.692 ± 0.023	-0.0162 ± 0.0033	0.99980
Mg	2.24 ± 0.34	-2.03 ± 0.24	-0.154 ± 0.040	0.9983
Al	-0.854 ± 0.133	-1.399 ± 0.023	-0.061 ± 0.021	0.99941
Si	-0.287 ± 0.039	-1.060 ± 0.030	-0.0470 ± 0.052	0.99986
P	-0.073 ± 0.028	-0.910 ± 0.019	-0.0448 ± 0.0029	0.99988
S	0.138 ± 0.031	-0.851 ± 0.021	-0.0450 ± 0.0031	0.99979
Cl	0.281 ± 0.025	-0.706 ± 0.015	-0.0355 ± 0.0018	0.99981
Ca	-2.13 ± 0.20	-1.82 ± 0.14	-0.069 ± 0.023	0.99981
Sc	-2.75 ± 0.12	-2.337 ± 0.084	-0.168 ± 0.014	0.99992
Ti	-1.862 ± 0.087	-1.762 ± 0.059	-0.0879 ± 0.0096	0.99994
V	-1.143 ± 0.050	-1.340 ± 0.034	-0.0310 ± 0.0055	0.99998
Cr	0.275 ± 0.094	-0.737 ± 0.094	-0.0424 ± 0.0091	0.99989
Mn	-0.898 ± 0.052	-1.187 ± 0.035	-0.0167 ± 0.0055	0.99997
Fe	0.29 ± 0.10	-0.442 ± 0.063	0.0732 ± 0.096	0.99983
Co	0.362 ± 0.088	-0.362 ± 0.055	-0.0884 ± 0.0083	0.99987
Ni	0.31 ± 0.11	-0.375 ± 0.069	0.0860 ± 0.0103	0.99980
Cu	0.15 ± 0.14	-0.441 ± 0.083	0.077 ± 0.012	0.99974
Zn	-0.703 ± 0.068	-1.087 ± 0.041	-0.0276 ± 0.0061	0.99992
Ga	-0.523 ± 0.060	-1.161 ± 0.043	-0.0228 ± 0.0074	0.99993
Ge	-0.324 ± 0.053	-1.083 ± 0.035	-0.0450 ± 0.0053	0.99989
As	-0.151 ± 0.034	-0.966 ± 0.020	-0.0455 ± 0.0027	0.99993
Se	0.042 ± 0.023	-0.941 ± 0.014	-0.0509 ± 0.0018	0.99995
Br	0.154 ± 0.025	-0.830 ± 0.014	-0.0422 ± 0.0017	0.99993

The errors correspond to 95% confidence intervals and $\mathcal{C}$ is the correlation coefficient. For C–Cl, we used 11 points between $r = 1.0$ Å and 3.5 Å. For Ca–Br, we used 10 points between $r = 1.5$ Å and 3.75 Å.

distinguished in terms of size. From Figure 7, the boundary of this region is defined by $\rho \sim 0.01$ a.u. and $r \approx R_{core} \sim 1.3$ Å (denoted by 'Core' in the figure). The present results indicate that this core is *always* inside the van der Waals spheres. Moreover, Figure 7 shows that different atoms appear to have different atomic spheres *only* when we reach the range of electron density chosen as reference, i.e., $\rho \approx 0.0036 \pm 0.0010$ a.u. (denoted by 'Boundary' in the figure). Within this boundary, we can recognize the effect of the *d*-electrons on the atomic radius. Outside the boundary (i.e., the region denoted by 'Exterior' in the figure), there is little qualitative change in the ordering of the atomic radii along the transition metal series.

The above results indicate an interesting property: our chosen 'reference' electron density boundary coincides always with an electron shell just outside the invariant core. Note that the general reference ρ value is determined by fitting to a *single* van der Waals empirical radius (that of carbon). However, the resulting ρ value leads consistently to atomic spheres located outside the electron core for all tested elements. This finding explains the partial success of the large-core approximation for computing atomic radii. In addition, the present analysis supports the notion that fused-sphere models can be regarded as an approximation to isodensity surfaces. Our results show that the standard van der Waals radii define a region of space around an atom where the one-electron density has a rather uniform value, regardless of the element considered.

Acknowledgements

We would like to acknowledge many enjoyable and inspiring discussions with Paul Mezey (Saskatchewan) over the years on the subject of the molecular shape of electron isodensity surfaces. G.A.A. thanks Roy

Kari (Laurentian) for lending his fitting program XLQChem. This work was supported by grants from NSERC (Canada) and FRUL (Laurentian).

References

1. Richards, F.M., Annu. Rev. Biophys. Bioeng., 6 (1977) 151.
2. Mezey, P.G., In Lipkowitz, K.B. and Boyd, D.B. (Eds.), Reviews in Computational Chemistry, Vol. 1, VCH Publishers, New York, NY, 1990, pp. 265–294.
3. Brinck, T., Murray, J.S. and Politzer, P., Mol. Phys., 76 (1992) 609.
4. Bader, R.F.W., Atoms in Molecules, Clarendon Press, Oxford, 1990.
5. a. Yang, W., Phys. Rev. Lett., 66 (1991) 1438.
   b. Yang, W. and Lee, T.-S., J. Chem. Phys., 103 (1995) 5674.
6. Walker, P.D., Arteca, G.A. and Mezey, P.G., J. Comput. Chem., 12 (1991) 220.
7. Grant, J.A. and Pickup, B.T., J. Phys. Chem., 99 (1995) 3503.
8. a. Walker, P.D. and Mezey, P.G., J. Am. Chem. Soc., 115 (1993) 12423.
   b. Walker, P.D. and Mezey, P.G., J. Am. Chem. Soc., 116 (1994) 12022.
9. Mezey, P.G., Shape in Chemistry, VCH Publishers, New York, NY, 1993.
10. Ooi, T., Oobatake, M., Némethy, G. and Scheraga, H.A., Proc. Natl. Acad. Sci. USA, 84 (1987) 3086.
11. Abraham, M.H., Chem. Soc. Rev., 22 (1993) 73.
12. a. Tuñón, I., Silla, E. and Pascual-Ahuir, J.L., Protein Eng., 5 (1992) 715.
    b. Tuñón, I., Silla, E. and Pascual-Ahuir, J.L., Chem. Phys. Lett., 203 (1993) 289.
13. Hansch, C. and Leo, A., Exploring QSAR, American Chemical Society, Washington, DC, 1995.
14. Mebane, R.C., Williams, C.D. and Rybolt, T.R., Fluid Phase Eq., 124 (1996) 111.
15. Politzer, P., Parr, R.G. and Murphy, D.R., J. Chem. Phys., 79 (1983) 3859.
16. Bader, R.F.W., Carroll, M.T., Cheeseman, J.R. and Chang, C., J. Am. Chem. Soc., 109 (1987) 7968.
17. Arteca, G.A., Grant, N.D. and Mezey, P.G., J. Comput. Chem., 12 (1991) 1198.
18. a. Ganguly, P., J. Am. Chem. Soc., 115 (1993) 9287.
    b. Ganguly, P., J. Am. Chem. Soc., 117 (1995) 2655.
19. García, A. and Cohen, M.L., Phys. Rev. B, 47 (1993) 4221.
20. Fernández Pacios, L., J. Comput. Chem., 16 (1995) 133.
21. Chattaraj, P.K., Cedillo, A. and Parr, R.G., J. Chem. Phys., 103 (1995) 10621.
22. Ghanty, T.K. and Ghosh, S.K., J. Phys. Chem., 100 (1996) 17429.
23. Du, Q. and Arteca, G.A., J. Comput. Chem., 17 (1996) 1258.
24. Gibbs, G.V., Tamada, O. and Boisen Jr., M.B., Phys. Chem. Minerals, 24 (1997) 432.
25. Yang, Z.-Z. and Davidson, E.R., Int. J. Quantum Chem., 62 (1997) 47.
26. Krauss, M. and Stevens, W.J., Annu. Rev. Phys. Chem., 35 (1984) 357.
27. Frenking, G., Antes, I., Böhme, M., Dapprich, S., Ehlers, A.W., Jonas, V., Neuhaus, A., Otto, M., Stegmann, R., Veldkamp, A. and Vyboishchikov, S.F., In Lipkowitz, K.B. and Boyd, D.B. (Eds.), Reviews in Computational Chemistry, Vol. 8, VCH Publishers, New York, NY, 1996, pp. 63–143.
28. Cundari, T.R., Benson, M.T., Lutz, M.L. and Sommerer, S.O., In Lipkowitz, K.B. and Boyd, D.B. (Eds.), Reviews in Computational Chemistry, Vol. 8, VCH Publishers, New York, NY, 1996, pp. 145–202.
29. Ganguly, P., J. Am. Chem. Soc., 117 (1995) 1777.
30. a. Zunger, A. and Cohen, M.L., Phys. Rev. B, 18 (1978) 5449.
    b. Zunger, A. and Cohen, M.L., 20 (1979) 4082.
31. Frisch, M.J., Trucks, G.W., Head-Gordon, M., Gill, P.M.W., Wong, M.W., Foresman, J.B., Johnson, B.G., Schlegel, H.B., Robb, M.A., Replogle, E.S., Gomperts, R., Andrés, J.L., Raghavachari, K., Binkley, J.S., González, C., Martin, R.L., Fox, D.J., Defrees, D. J., Baker, J., Stewart, J.J.P. and Pople, J.A., Gaussian 92 (Revision G.4), Gaussian, Inc., Pittsburgh, PA, 1992.
32. Hay, J.P. and Wadt, W.R., J. Chem. Phys., 82 (1985) 270.
33. Hay, J.P. and Wadt, W.R., J. Chem. Phys., 82 (1985) 299.
34. Bettega, M.H.F., Natalense, A.P.P., Lima, M.A.P. and Ferreira, L.G., Int. J. Quantum Chem., 60 (1996) 821.
35. Stevens, W.J., Krauss, M., Basch, H. and Jasien, P.G., Can. J. Chem., 70 (1992) 612.
36. Cundari, T.R., J. Am. Chem. Soc., 114 (1992) 7879.
37. a. Cundari, T.R. and Stevens, W.J., J. Chem. Phys., 98 (1993) 5555.
    b. Cundari, T.R., Sommerer, S.O. and Stevens, W.J., Chem. Phys., 178 (1993) 235.
38. Vyboishchikov, S.F., Sierraalta, A. and Frenking, G., J. Comput. Chem., 18 (1996) 416.
39. Bondi, A., J. Phys. Chem., 68 (1964) 441.
40. Gavezzotti, A., J. Am. Chem. Soc., 105 (1983) 5220.
41. Pauling, L., The Nature of the Chemical Bond, Cornell University Press, Ithaca, NY, 1960.
42. Weast, R.C. (Ed.), CRC Handbook of Chemistry and Physics, CRC Press, Boca Raton, FL, 1988, p. D-111.